

A Realistic Radar Simulation Framework for CARLA

Anonymous CVPR submission

Paper ID 12354

Abstract

001 *The advancement of self-driving technology has become*
002 *a focal point in outdoor robotics, driven by the need for*
003 *robust and efficient perception systems. This paper ad-*
004 *resses the critical role of sensor integration in autonomous*
005 *vehicles, particularly emphasizing the underutilization of*
006 *radar compared to cameras and LiDARs. While extensive*
007 *research has been conducted on the latter two due to the*
008 *availability of large-scale datasets, radar technology offers*
009 *unique advantages such as all-weather sensing and occlu-*
010 *sion penetration, which are essential for safe autonomous*
011 *driving. This study presents a novel integration of a realistic*
012 *radar sensor model within the CARLA simulator, enabling*
013 *researchers to develop and test navigation algorithms us-*
014 *ing radar data. Utilizing this radar sensor and showcas-*
015 *ing its capabilities in simulation, we demonstrate improved*
016 *performance in end-to-end driving scenarios. Our findings*
017 *aim to rekindle interest in radar-based self-driving research*
018 *and promote the development of algorithms that leverage*
019 *radar’s strengths.*

020 1. Introduction

021 Autonomous systems, especially self-driving cars, rely on
022 end-to-end pipelines that seamlessly connect perception to
023 downstream tasks like path planning and navigation. While
024 robust perception is a critical component of these systems,
025 the focus in end-to-end approaches is on ensuring that sensor
026 data directly informs actionable decisions. Multimodal
027 sensor fusion plays a pivotal role in this context, enabling
028 a holistic understanding of the environment by integrat-
029 ing complementary inputs from camera, LiDAR and radar
030 [8, 18]. This fusion enhances the system’s resilience to
031 varying conditions- radar excels in detecting speed and distance
032 in adverse weather, while camera offers detailed visual
033 information for interpreting road signs and traffic signals
034 [25].

035 Making multimodal sensors work well together also re-
036 quires a detailed understanding of how each sensor oper-

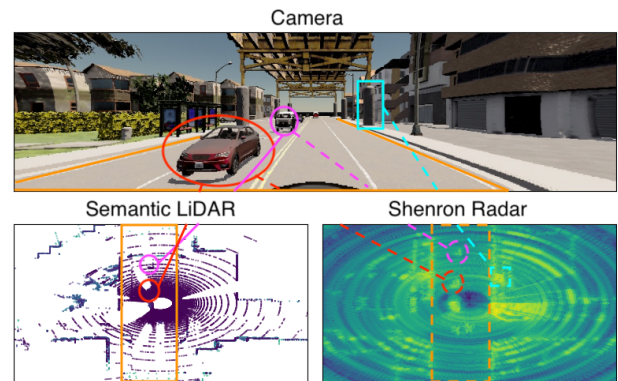


Figure 1. Comparison of views from Camera, Semantic LiDAR, and Shenron Radar in CARLA. The orange lines outline the road, red and magenta highlights vehicles, and blue indicates a static object.

037 ates, including their strengths, limitations, and behavior under
038 different conditions. Expanding on this understanding, a
039 fundamental question lies in determining what the right
040 configuration and placement of sensors are, enabling low
041 cost while ensuring robust performance and appropriate
042 sensor fusion algorithms to enable safe perception, nav-
043 igation, and path planning. Building all different config-
044 urations and hardware to achieve these objectives is im-
045 possible, highlighting the need for simulation tools. In ad-
046 dition, training such perception models for autonomous driv-
047 ing requires significant amounts of data encompassing vari-
048 ous scenarios to ensure reliable performance under different
049 conditions [2, 12, 17, 20]. A key challenge here is large-
050 scale data collection, as collecting data for every possible
051 situation is nearly impossible. Moreover, the collected data
052 is significantly impacted by the way the sensors are placed
053 and their specific characteristics. This challenge empha-
054 sizes the potential of simulations to enhance real-world data
055 collection.

056 The CARLA simulator excels in enabling both percep-
057 tion and downstream tasks in autonomous driving research.
058 It facilitates large-scale data collection by generating di-

059	verse datasets that capture a wide range of scenarios, includ-	CARLA simulator. We are also the first to generate high	112
060	ing varying weather conditions and complex traffic environ-	quality radar data across various towns and scenarios, utiliz-	113
061	ments [11]. CARLA supports end-to-end training pipelines	ing Kubernetes for automation and scaling. The data gener-	114
062	by providing accurate simulation of key sensors like camera	ated from the integrated radar sensors and camera was then	115
063	and LiDAR, making it an effective digital twin for the	utilized to train a state-of-the-art model [16], improving the	116
064	rapid development and testing of autonomous systems [1].	perception capabilities of the framework. This comprehen-	117
065	Researchers have extensively utilized CARLA to train per-	sive training showcased the benefits of multimodal fusion	118
066	ception models and integrate them into downstream tasks	to achieve accurate and reliable driving in a realistic simu-	119
067	like path planning and navigation, as noted in works such as	lation.	120
068	[7, 8, 16]. The simulator’s flexibility and precision have so-	We evaluated the end-to-end model in diverse driving	121
069	lidified its role as a vital tool for testing and validating state-	scenarios in a simulated environment. Using the simula-	122
070	of-the-art approaches, particularly in systems that leverage	tor allowed us to position various radars on the vehicle to	123
071	multi-modal fusion to achieve robust and reliable perfor-	identify the optimal setup for driving performance. An-	124
072	mance.	other significant challenge was to integrate multiple radar	125
073	While LiDAR is a useful sensor, it struggles with all-	views to achieve one 360° radar image to provide compre-	126
074	weather sensing due to its reliance on lasers. In contrast,	hensive situational awareness. We implemented a masking	127
075	radar employs millimeter-wave technology and is highly ef-	procedure to stitch these views together which enhanced our	128
076	fective in various conditions[3]. However, the radar model	model’s situational awareness. We also evaluate of each	129
077	in the CARLA simulator has significant limitations. Unlike	radar view’s utility through a redaction process, ensuring	130
078	real-world radar systems that utilize multiple radar beams,	the model accurately interpreted the combined radar infor-	131
079	advanced Doppler processing, and sophisticated clutter fil-	mation. Our results highlight that radar and camera-based	132
080	tering, CARLA’s radar is a simplified version that lacks	models achieve better performance in some scenarios and	133
081	these essential features. It generates data by randomly sam-	comparable performance in others, compared to traditional	134
082	pling LiDAR outputs, failing to capture key radar-specific	camera and LiDAR models.	135
083	characteristics, such as sensitivity to motion and environ-	The remainder of the paper is structured as follows:	136
084	mental influences. Additionally, there have been multiple	we review related work, discuss how radar enhances au-	137
085	velocity computation issues, with moving vehicles display-	tonomous driving reliability alongside CARLA, detail the	138
086	ing inaccurate speed readings [10]. These shortcomings	design and implementation of our approach, and conclude	139
087	render any research involving CARLA radar inadequate, as	with evaluations and future work proposals.	140
088	it does not reflect the real-world capabilities of an opera-		
089	tional radar sensor that can be used in autonomous vehicles	2. Related Work	141
090	[21].		
091	In this paper, we present C-Shenron, an innovative radar	The development of sensor technologies for autonomous	142
092	sensor model integrated into the CARLA simulator, exten-	driving has predominantly focused on vision-based and	143
093	ding the Shenron framework, which previously focused	LiDAR-based perception systems, attributed to their high-	144
094	solely on LiDAR data [4]. C-Shenron allows users to	resolution capabilities and the availability of extensive	145
095	configure and simulate diverse radar setups with different	datasets.	146
096	number of antenna arrays, thereby enabling comprehensive	Vision-Based Perception: Camera-based approaches	147
097	multi-modal data collection and simulation for end-to-end	have gained widespread adoption for tasks such as object	148
098	autonomous driving tasks. With C-Shenron, researchers	detection, lane detection, and scene understanding. The	149
099	can experiment with various radar sensor placements, ex-	success of these methods is largely due to the availability of	150
100	plorer multiple fusion strategies, and generate high-fidelity	large-scale datasets like KITTI, Cityscapes, and nuScenes,	151
101	datasets for training and testing robust perception models.	which facilitate the training of robust computer vision mod-	152
102	To achieve seamless functionality, we designed a server-	els [13]. These datasets have enabled rapid advancements	153
103	side sensor in CARLA that aggregates required data from	in visual perception algorithms, leveraging deep learning ar-	154
104	the simulation world into a unified stream, enabling efficient	chitectures to achieve high accuracy in identifying objects,	155
105	radar data generation and fusion with Shenron existing ca-	detecting obstacles, and recognizing traffic signs and sig-	156
106	pabilities. This innovation bridges the gap between CARLA	nals [9].	157
107	and Shenron, establishing a cohesive platform for advanc-	LiDAR-Based Perception: LiDAR technology is also	158
108	ing radar-based multimodal fusion research in autonomous	prevalent in autonomous vehicle research due to its precise	159
109	driving research.	depth information and accurate 3D mapping capabilities.	160
110	To demonstrate the functionality of this new sensor, we	This allows for complex tasks such as 3D object detection	161
111	gathered data, trained, and evaluated the model within the	and point-cloud segmentation. Significant advancements in	162
		LiDAR-based perception have been supported by dedicated	163

164	datasets like the Waymo Open Dataset and SemanticKITTI	217
165	[22]. These resources, combined with LiDAR’s ability to	218
166	capture detailed 3D spatial information, have made it a pre-	219
167	ferred choice for high-resolution sensing in self-driving sys-	220
168	tems. However, LiDAR performance can degrade in ad-	221
169	verse weather conditions and struggles with occlusion pen-	
170	etration, posing challenges in real-world scenarios [5].	
171	Radar-Based Perception: Radar technology has	
172	emerged as a crucial component in the sensor suite for au-	
173	tonomous vehicles. Sensor fusion techniques have been piv-	
174	otal in enhancing radar-based perception by integrating data	
175	from multiple sensors, including lidar and cameras. This	
176	multi-modal approach leverages the strengths of each sen-	
177	sor type to improve detection accuracy and robustness [8].	
178	Studies have shown that fusing radar data with visual infor-	
179	mation can significantly enhance performance in complex	
180	driving scenarios by providing complementary information	
181	that addresses individual sensor limitations [22].	
182	A novel approach proposed by Kshitiz et al. [3] enhances	
183	radar-based perception by employing multiple radar units to	
184	generate accurate 3D bounding boxes for object detection.	
185	Another work by Kshitiz et al. [4] laid the groundwork for	
186	developing realistic radar sensing models, which we extend	
187	in this paper to enhance the CARLA simulator. However,	
188	challenges remain, such as dealing with sparse data and op-	
189	timizing algorithms to better interpret radar measurements	
190	under varying conditions. By integrating a high-fidelity	
191	radar model, we aim to open new avenues for self-driving	
192	algorithms that utilize radar data effectively.	
193	The CARLA simulator, which stands for CAR Learn-	
194	ing Algorithm, has facilitated numerous advances in au-	
195	tonomous driving research by providing robust support for	
196	various sensors[6, 7, 15, 19, 24]. However, the lack of real-	
197	istic radar sensor simulations within CARLA limits its util-	
198	ity for research focused on radar-based navigation [11].	
199	Multi-Modal Sensor Fusion: The introduction of the	
200	TransFuser model [8] in 2021 marked a significant step	
201	forward in multi-modal sensor fusion approaches for au-	
202	tonomous driving. Utilizing a transformer architecture	
203	for end-to-end driving policy development, TransFuser in-	
204	tegrates data from cameras and LiDAR to enhance per-	
205	formance in complex driving scenarios. By effectively	
206	combining these diverse sensor inputs, it addresses the	
207	limitations inherent to single-sensor approaches. Trans-	
208	Fuser++ [16] builds upon this foundation with improved	
209	sensor integration and advanced data augmentation tech-	
210	niques. It introduces cross-attention mechanisms that better	
211	align inputs from different sensors, addressing compound-	
212	ing errors in trajectory prediction. By incorporating up-	
213	dated training protocols and data handling strategies, Trans-	
214	Fuser++ achieves higher performance benchmarks, such as	
215	CARLA’s Longest6 and MAP leaderboard, demonstrating	
216	its capability to maintain route accuracy while reducing in-	
	fractions.	217
	This evolution underscores the potential of multi-sensor	218
	fusion approaches in designing more resilient autonomous	219
	driving systems that can integrate new sensors like radar to	220
	enhance perception and decision-making.	221
	3. Background	222
	3.1. Radar in Autonomous Driving	223
	In the real world, Camera and LiDAR are more commonly	224
	used in autonomous driving than radar due to radar’s incon-	225
	sistent standardization and its sensitivity to noise and lower	226
	resolution. However, Radar offers unique benefits com-	227
	pared to LiDAR and cameras, especially in adverse weather	228
	conditions. Unlike optical sensors, radar uses radio waves,	229
	allowing it to penetrate through rain, fog, snow, and dust,	230
	making it more reliable for all-weather performance. Its	231
	long-range detection capabilities, as noted in Table 1, sur-	232
	pass those of LiDAR and cameras, which is particularly use-	233
	ful in high-speed driving and congested environments. Ad-	234
	ditionally, radar’s ability to maintain low noise sensitivity	235
	and track velocity over long distances, as shown in Table 1,	236
	highlights its suitability for challenging driving scenarios.	237
	Radar’s doppler measurement capability, which provides in-	238
	formation on the relative velocity of objects, is crucial for	239
	tasks like path planning, trajectory prediction, and enhanc-	240
	ing spatial resolution.	241
	3.2. CARLA Sensors	242
	Sensors act as the eyes and ears of autonomous vehicles,	243
	making it crucial for the CARLA simulator to provide ac-	244
	curate and realistic sensor simulations. CARLA includes	245
	all the main sensors needed for autonomous driving such as	246
	camera, LiDAR, radar, GNSS (Global Navigation Satellite	247
	System), IMU (Inertial Measurement Unit) and many oth-	248
	ers. Furthermore CARLA includes sensors that are chal-	249
	lenging to access in real-world scenarios due to safety and	250
	logistical constraints, such as collision and lane invasion de-	251
	tectors, an odometer, and a Road Surface Sensor (RSS) that	252
	communicates traffic signals and lane markings.	253
	3.3. Unrealistic Qualities of CARLA Radar	254
	CARLA provides researchers with a unique opportunity to	255
	access high-quality multi-sensor data, which is often chal-	256
	lenging to obtain in real-world environments. However, the	257
	default radar sensor in CARLA has limitations that hinder	258
	its performance in tracking objects behind other vehicles	259
	and in long-range obstacle detection scenarios. It only pro-	260
	vides point cloud data for detection and tracking, lacking	261
	real-time velocity information, which is essential for accu-	262
	ately assessing object motion and ensuring safe navigation.	263
	While point cloud data allows precise mapping through 3D	264
	coordinates, the absence of velocity data forces reliance on	265

Sensor Type	Cost	Noise Sensitivity	Range	Resolution	Weather Resistance	Velocity Tracking	Height Tracking
Camera	✓	✓	●	✓	✗	✗	✗
LiDAR	✗	✗	✓	●	✗	●	●
Radar	✓	✓	✓	✗	✓	✓	✓

Table 1. Comparison of sensor types—Camera, LiDAR, and Radar—across various attributes. Green checkmarks indicate favorable traits, yellow circles indicate moderate traits, and red crosses indicate unfavorable traits.

266 historical position data, which can result in delayed reac-
 267 tions and reduced situational awareness. Furthermore, raw
 268 3D radar data provides a richer, more detailed representa-
 269 tion of the environment compared to traditional radar point
 270 cloud data, making it particularly valuable for applications
 271 in autonomous driving and advanced perception systems.
 272 Our proposed C-Shenron radar provides high-quality, accu-
 273 rate radar data.

274 4. Design

275 We integrate a new scalable, high-fidelity, and efficient
 276 radar (Shenron) sensor with the CARLA simulator. Shen-
 277 ron is an open-source framework that can simulate high-
 278 fidelity MIMO radar data using the information from the Li-
 279 DAR point clouds and camera images. It leverages the im-
 280 pulse response captured by LiDAR sensors, which provide
 281 a point cloud representation of the environment, to simu-
 282 late radar data without the need for complex geometries. To
 283 derive accurate radio frequency (RF) reflection profiles for
 284 various materials, the framework uses semantic information
 285 from the camera images. By combining both specular and
 286 scattering reflection models, Shenron achieves a high corre-
 287 lation with real-world radar data, making it a robust tool for
 288 evaluation of radar algorithms.[4].

289 Shenron requires lidar point cloud data, along with se-
 290 mantic tags and the relative velocity of those points con-
 291 cerning the sensor, as input to generate raw 3D radar data,
 292 which includes range, angle, and doppler dimensions. The
 293 new sensor we introduce on the server side of CARLA ful-
 294 fills these requirements by providing the necessary data. It
 295 is then utilized by Shenron to produce comprehensive 3D
 296 radar outputs, enhancing the fidelity of radar data in au-
 297 tonomous driving simulations.

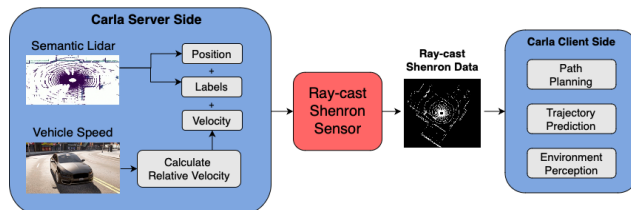


Figure 2. C-Shenron as the Shenron integration in CARLA

298 4.1. Challenges in integrating Shenron within 299 CARLA

300 Sensors in CARLA follow a pipeline that transforms the
 301 raw sensor data into a usable format. Each sensor type is
 302 represented as a special actor within the simulation. The
 303 sensor actor interacts with the simulated environment and
 304 continuously gathers data based on its type and configura-
 305 tion.

306 CARLA operates on a client-server architecture, where
 307 the server simulates the virtual world and the client applica-
 308 tion interacts with this simulated environment. The server
 309 handles the physics simulation, traffic management, and
 310 sensor data generation. It also manages the communication
 311 with the client, transmitting sensor data and receiving con-
 312 trol inputs from the client. The client application, typically
 313 written in Python, receives sensor data from the server, pro-
 314 cesses it, and sends control commands back to the server.
 315 Sensors in CARLA retrieve data either at every simulation
 316 step or when the specific event occurs. For example, the
 317 camera generates images at every frame, whereas collision
 318 sensors are activated upon detecting an event. The collected
 319 raw sensor data, along with metadata such as sensor type,
 320 frame number and timestamp, is serialized and transmitted
 321 to the client application via a real time communication pro-
 322 tocol.

323 On the client side, applications can subscribe to a sen-
 324 sor’s data stream. When a new data frame arrives, a reg-
 325 istered callback function is triggered. This function dese-
 326 rializes the data stream back into a SensorData object and
 327 processes it further. This modular design allows for the in-
 328 tegration of the custom sensors. However, the core sensor
 329 actor, data stream, and server to client communication are
 330 implemented in C++ using specific data structures and func-
 331 tions.

332 4.2. C-Shenron

333 To seamlessly integrate the Python-based Shenron sensor
 334 into the C++-based CARLA simulation environment, we
 335 devised a hybrid approach that addresses the fundamen-
 336 tal challenges posed by this integration. We introduced a
 337 custom C++ Raycast Shenron sensor on the server side to
 338 capture point cloud data, including semantic segmentation
 339 and relative velocity information. This approach aligns with

340 CARLA’s native C++ architecture, ensuring efficient com-
341 munication and integration with the core simulation loop.
342 The data collected by the Raycast Shenron sensor along
343 with metadata is then transmitted to the client side. On
344 the client side, Shenron processes the received data to gen-
345 erate the simulated radar data. To mitigate the real-time
346 latency introduced by the Shenron processing, we paused
347 the CARLA simulation during this phase, ensuring that the
348 overall simulation time remains unaffected. The Figure
349 2 represents the overall picture of the Shenron integration
350 with CARLA.

351 4.2.1. Relative Velocity Calculation

352 We implement the functions required to calculate the rela-
353 tive velocity in our new Raycast Shenron sensor. We com-
354 pute the relative velocity v_{rel} of a detected target relative to
355 the Raycast Shenron sensor, \mathbf{v}_s . It retrieves the target’s ve-
356 locity, \mathbf{v}_t , and calculates the normalized direction vector, \mathbf{d} ,
357 from the Raycast Shenron sensor to the target. By finding
358 the velocity difference between the target and the sensor and
359 taking the dot product with this direction vector, the func-
360 tion isolates the component of relative velocity along the
361 line connecting the sensor and the target. This result, repre-
362 sents the target’s velocity relative to the Raycast Shenron,

$$363 v_{rel} = (\mathbf{v}_t - \mathbf{v}_s) \cdot \mathbf{d}$$
$$364 \mathbf{d} = \frac{\mathbf{p}_t - \mathbf{p}_s}{\|\mathbf{p}_t - \mathbf{p}_s\|}$$

365

366 where \mathbf{p}_t and \mathbf{p}_s are the position vectors of the sensor and
367 target respectively.

368 4.2.2. Dense Point Cloud Generation

369 To generate a dense point cloud data with a complete 360-
370 degree field of view at each simulation step, we concate-
371 nated two 180-degree frames, aligning the previous frame
372 with the current ego-vehicle position. By capturing two
373 half-frames and combining them, we effectively doubled
374 the point cloud density, resulting in a more accurate and de-
375 tailed representation of the surrounding environment. This
376 approach was crucial to generate realistic radar signals.

377 We developed a comprehensive solution that facilitates
378 the integration of Shenron sensor into the CARLA system
379 seamlessly. Additionally, we provide example scripts to
380 simulate and visualize the Shenron radar data within the
381 CARLA environment, demonstrating how to effectively use
382 this radar in your simulations. Detailed instructions and
383 resources are available as open source on the following
384 GitHub repository: CARLA-Shenron-release.

385 5. Implementation

386 In this section we’ll dive into how we utilized integrated
387 Shenron in CARLA to train a end-to-end Perception and

Driving model, built on top of the Transfuser++ architecture
[16].

5.1. End-to-end driving with CARLA Garage

Safe navigation is the ultimate goal of a self-driving car,
which includes identifying obstacles, planning the path
around them and eventually reaching the goal. Integrating
a realistic sensor model in CARLA gives us the ability to
test the effect of radar algorithms on downstream tasks like
path planning and navigation. Hence we use this opportu-
nity to perform extensive experimentation on the effect of
using radar data on downstream tasks. In this section we
first describe the end-to-end driving system used for percep-
tion and planning followed by the results obtained when we
evaluated navigation performance achieved by using radar.

5.1.1. CARLA Garage

We use the CARLA Garage [14] platform for generation
of high-quality data and training of end-to-end autonomous
driving models. The platform provides supports integra-
tion and deployment of both pretrained and custom models,
offering necessary scripts and tools for dataset generation,
model training, and benchmark evaluations, thus stream-
lining the process. Through this platform, we customized
across multiple sensor placements and input data for train-
ing the end-to-end Deep Learning model of our choice. The
output of the model is used as control signals for actions
such as steering, brakes and gas that can be used to drive a
autonomous agent in the simulation.

5.2. Dataset Generation

CARLA employs an expert autonomous agent that emulates
driving of an experienced human driver, producing highly
reliable driving data which is essential for training large au-
tonomous driving models. This expert agent follows prede-
fined traffic rules, navigates traffic scenarios, and interacts
safely with obstacles just like an experienced human driver
would perform. This expert also has direct access to de-
tailed map data like lane boundaries, traffic signals, speed
limits, and waypoints, enabling precise route planning and
rule compliance without relying on raw sensor interpreta-
tion. Additionally, the expert bypasses complex object de-
tection, directly retrieving the exact locations, velocities,
and classifications of vehicles, pedestrians, and obstacles,
thereby eliminating perception errors and ensuring reliable
tracking. Furthermore, it has perfect localization within the
environment, sidestepping common errors in real-world lo-
calization methods like GPS and LiDAR. This access to pre-
cise data enables the generation of a robust, high-quality
dataset, ideal for training and benchmarking autonomous
systems in controlled simulations.

To accelerate data collection, we launch multiple
CARLA instances in parallel, allowing simultaneous data
generation across various scenarios and weather conditions.

439 This approach enhances the dataset’s diversity and richness, reducing the collection time from days to hours. Using a Kubernetes cluster, we launch 210 jobs, each corresponding to a distinct CARLA instance for different route-scenario combinations across all 8 CARLA towns (Town01-Town07 and Town10), reserving Town08 and Town09 for evaluation. This results in 70 unique combinations, with each combination repeated thrice, yielding a total of 555k frames. For our experiments, we only train the model on 185k frames, excluding repetitions. The additional data gathered may be utilized in future experiments to assess the impact of a larger training dataset on model performance. We will also release the complete collected dataset for the research community.

453 5.3. Integrating with TF++ Architecture

454 In CARLA Garage, we employ Transfuser++, a state-of-the-art model, for both perception and planning tasks. The Transfuser++ architecture features a transformer-based sensor fusion module that integrates camera and LiDAR data, alongside auxiliary branches for perception tasks like classification, detection, and segmentation. In our evaluations, we don’t utilize any of these auxiliary branches and only use the Transformer encoders and decoders. Additionally, it includes a transformer decoder to output the target speed and path for the autonomous vehicle. For more details on the architecture, refer to [16]. In our implementation, we create high-fidelity radar data from Shenron as range-angle plots and input these images directly into the BEV branch, bypassing the LiDAR images as seen in Figure 3, and further conduct end-to-end training and evaluation of this model.

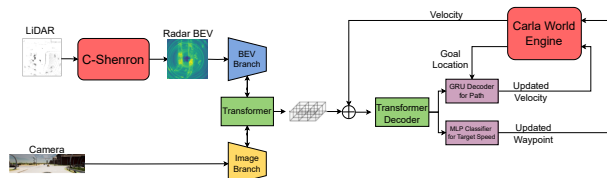


Figure 3. C-Shenron with the Transfuser++ Architecture

469 5.4. Training details

470 To train our model, we adopted the same loss function employed in the Transfuser++ architecture [16]. Our training process involved a batch size of 12 and 30 epochs. We utilized a learning rate of 3×10^{-4} , and trained the model on a system equipped with 6 NVIDIA A10 GPUs, which required approximately 2 days to complete the training process.

477 6. Evaluation

478 In this section, we evaluate our trained model, which incorporates the Shenron sensor system, by comparing its driv-

ing performance with that of current state-of-the-art end-to-end driving models. Our primary model for processing autonomous vehicle sensor data is Transfuser++ [16]. We also present two case studies that explore varying radar sensor placements and assess the impact of these configurations. Our results indicate that radar images can serve as an effective alternative to LiDAR, delivering comparable performance along with enhanced all-weather capability. These results reopen the field for utilizing radars in end-to-end autonomous driving.

490 6.1. Metrics

491 The driving proficiency of an autonomous agent is evaluated through various metrics provided by CARLA that gives insights into different aspects of driving behavior. In the context of our setup, we evaluate on a set of metrics that offers a comprehensive understanding of the agent’s performance. The specific metrics are :-

- 497 • **Driving Score:** The primary metric of the leaderboard, calculated as the product of the other two metrics: route completion and the infractions penalty. 498 499
- 500 • **Route completion:** It is the percentage of the route distance completed by an agent. 501
- 502 • **Infraction Penalty:** The leaderboard tracks multiple types of infractions, and this metric consolidates all infractions triggered by an agent into a single score, calculated as a geometric series. 503 504 505

506 In the CARLA simulation, infractions are penalized based on severity. For example, collisions with pedestrians, vehicles, and static objects incur varying penalties. Traffic violations, such as running red lights or stop signs, also result in higher penalties. Indefinite blockage of the vehicle leads to a timeout and additional penalties. 507 508 509 510 511

512 Agents must adhere to surrounding traffic speeds and yield to emergency vehicles, with noncompliance resulting in further penalties. Driving off-road negatively affects the route score, as that segment is excluded. Certain events, like significant deviations from the route or prolonged inactivity, can lead to a simulation shutdown. Each of these incidents is meticulously recorded, providing comprehensive insights into the performance of the agent throughout the simulation [23]. Once all routes are completed, an overall metric for each of the three types is calculated by taking the arithmetic mean of all individual route metrics combined. 513 514 515 516 517 518 519 520 521 522

523 6.2. Case Studies

524 We evaluate our models using the routes from NEAT [7] paper, which include various settings like highways, urban areas, and residential zones with diverse road layouts and obstacles to simulate urban conditions. Agents face traffic scenarios based on NHTSA typology, such as navigating intersections, responding to pedestrians, cyclists, and other road users, and many more. To ensure consistency, each 525 526 527 528 529 530

531 model was tested on the same set of 14 routes over 5
532 iterations under stable, moderate conditions without extreme
533 weather. Additionally, we carried out two case studies to
534 examine the impact of different sensor placements and the
535 impact of each radar view on performance in end-to-end
536 driving tasks.

537 6.2.1. Does increasing radar views help?

538 In this case study we analyze the potential benefits of in-
539 creasing the number of radar views on our autonomous ve-
540 hicle. The Shenron radar generated from combining camera
541 and LiDAR offers a 180° field of view (FOV), but the image
542 quality decreases as the coverage angle widens. We evaluate
543 three configurations of our radar models: front only radar,
544 front and back radars, and full coverage with front, back,
545 left, and right radars (we will denote as FBLR). All confi-
546 gurations are also fused with camera features. Note that all
547 the views of radar have 180° FOV.

548 When using front and back radar views, combining them
549 is straightforward; the two can simply be concatenated ver-
550 tically to create a complete 360° image, as illustrated in
551 Figure 4a. However, an interesting challenge arises when
552 attempting to merge the four radar views into a single high-
553 quality image. A basic method would be to extract 90° FOV
554 from each image and arrange them in a circular pattern, but
555 this approach is inefficient. Shenron-generated radar im-
556 ages contain concentric circular lines with slightly varying
557 radii, depending on the view, resulting in diagonal lines and
558 irregular patterns across the combined radar image, which
559 impairs perception. This can also be seen in Figure 4a,
560 where a horizontal line is present in the middle of the image.

561 An alternative approach involves overlapping of border
562 regions from different views to average out this inconsis-
563 tency. This technique uses a specialized mask as seen in
564 Figure 4b which are then rotated for proper orientation and
565 combined through pixel-wise addition. The mask’s magni-
566 tude decreases linearly before the $\pm 45^\circ$ line and drops to
567 0 beyond the line, which compensates for brightness varia-
568 tion in the overlapping regions when performing pixel-wise
569 addition. The resulting composite radar image Figure 4c
570 demonstrates the efficacy of this approach and creates an
571 accurate representation of the vehicle’s surroundings.

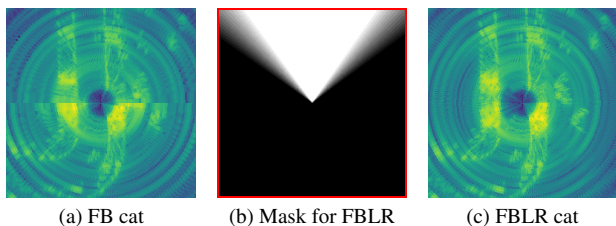


Figure 4. Images representing: (a) Radar image after Front+Back concatenation, (b) Mask for FBLR concatenation, (c) Radar image after FBLR concatenation.

572 The findings are presented in Table 2. LiDAR serves as
573 the baseline for comparison, being the original version of
574 Transfuser++ retrained on the collected LiDAR and Camera
575 data using the same parameters. Among the radar models,
576 the Front+Back configuration demonstrates the best perfor-
577 mance across all metrics, significantly outperforming the
578 LiDAR model (+6 in DS and +0.05 in IS). The Front-only
579 radar model also surpasses LiDAR, indicating that a single
580 radar view can exceed the baseline performance. Notably,
581 the FBLR configuration has a lower DS than Front+Back,
582 likely due to its low RC score; however, it exhibits more sta-
583 bility and lower variance, suggesting that additional field-
584 of-view sensors enhance consistency.

Radar View	DS \uparrow	RC \uparrow	IS \uparrow
LiDAR (ours)	76.84 \pm 5.26	95.93 \pm 3.43	0.79 \pm 0.05
Front	79.97 \pm 5.36	96.52 \pm 3.02	0.82 \pm 0.06
Front+Back	82.39 \pm 4.87	97.03 \pm 2.95	0.84 \pm 0.03
FBLR	79.24 \pm 1.85	93.56 \pm 2.75	0.84 \pm 0.05
Expert	93.82	97.394	0.964

Table 2. Results for different radar views with Driving Score (DS), Route Completion (RC) and Infraction Score (IS).

585 Lastly, the Expert model represents statistics from
586 CARLA’s driver agent, which sets a theoretical upper per-
587 formance limit as its training data was derived from this
588 agent. Although none of the models achieve expert per-
589 formance, the Front+Back radar configuration is the closest
590 across all metrics. Overall, radar-based models outperforms
591 the Camera + LiDAR setups in all key areas.

592 Looking deeper into driving scores from Figure 5, in
593 Urban routes, Front+Back performed slightly better than
594 FBLR, suggesting rear radar coverage is beneficial in con-
595 gested traffic. On Highways, FBLR greatly outperformed
596 the others, which outlines the importance of 360-degree
597 radar for detecting vehicles from multiple directions. Over-
598 all, additional radar views enhance performance across
599 routes, with the greatest impact on highways.

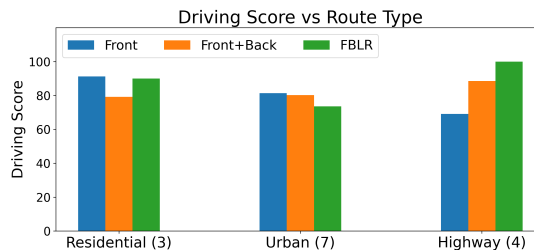


Figure 5. Route-wise Driving Score for Multiple Radar Views. The three categories have 3, 7 and 4 routes respectively.

600 Table 3 presents other scores where the FBLR configura-
601 tion excels in detecting vehicular collisions, static objects,
602 and route deviations, while the Front+Back configuration

603 performs best in red light infractions and agent timeouts.
 604 FBLR’s strong vehicle detection benefits from its multi-
 605 directional radar views, enhancing its ability to avoid obsta-
 606 cles (perfect score in static object detection). However, the
 607 Front+Back configuration minimizes red light infractions
 608 and completely avoids timeouts, suggesting that fewer in-
 609 puts simplify decision-making. In conclusion, FBLR is op-
 610 timal for environmental awareness, while Front+Back ex-
 611 cels in rapid decision-making situations, both surpassing
 612 driving performances by LiDAR.

Radar View	Veh ↓	Stat ↓	Red ↓	Dev ↓	TO ↓
LiDAR	0.62 ± 0.16	0.00	0.14 ± 0.09	0.02 ± 0.05	0.04 ± 0.04
Front	0.51 ± 0.21	0.06 ± 0.04	0.05 ± 0.06	0.06 ± 0.04	0.00
Front+Back	0.43 ± 0.12	0.01 ± 0.02	0.05 ± 0.04	0.01 ± 0.03	0.00
FBLR	0.32 ± 0.06	0.00	0.26 ± 0.10	0.00	0.09 ± 0.08
Expert	0.00	0.00	0.00	0.00	0.14

Table 3. Results for different radar views with Vehicle Infractions (Veh), Static Object Collisions (Stat), Red Light Infractions (Red), Route Deviations (Dev) and Agent Time Outs (TO).

6.2.2. Redaction of Radar views

613 To evaluate the utility of each radar sensor placements in
 614 the FBLR model, we conduct an ablation study where one
 615 of the four radar views are removed at a time and re-run the
 616 simulation for each configuration. This approach helps to
 617 assess the impact of each individual radar placement on the
 618 overall driving performance.
 619

Redact	DS ↑	RC ↑	IS ↑
Camera only	64.35	85.83	0.70
Left	75.79 ± 1.79	93.65 ± 2.68	0.78 ± 0.02
Right	76.61 ± 3.00	91.06 ± 0.91	0.82 ± 0.04
Front	35.88 ± 8.63	91.07 ± 3.66	0.37 ± 0.10
Back	73.30 ± 4.25	96.16 ± 3.80	0.77 ± 0.03
No Redact	79.24 ± 1.85	93.56 ± 2.75	0.84 ± 0.03

Table 4. Redaction of radar results with Driving Score (DS), Route Completion (RC) and Infraction Score (IS).

620 The results from the Table 4 indicate that, redacting the
 621 front view results in the most significant drop in perfor-
 622 mance suggesting that the front view is critical for obsta-
 623 cle detection and lane positioning. In contrast, redacting left or
 624 right views has a smaller impact on performance indicating
 625 that while these views contribute to lateral awareness, they
 626 are less crucial than the front view. Similar results are also
 627 observed for removing the back radar view as well. The
 628 camera only model performs the least across all the scores
 629 indicating that having radar views helps the model.

630 Route-wise scores from Figure 6 solidify the point of
 631 combining all four views gives for optimal situational
 632 awareness in the FBLR model. Throughout all routes, the
 633 redaction of front view consistently scores lower, suggest-
 634 ing it is very critical than other perspectives.

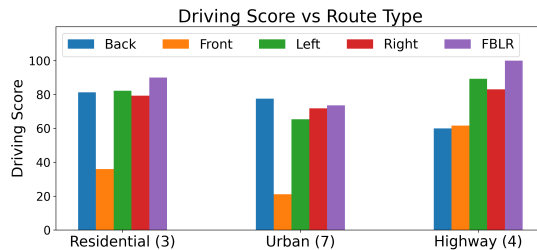


Figure 6. Route-wise Driving Score for Redaction of Radar. The three categories have 3, 7 and 4 routes respectively.

Redact	Veh ↓	Stat ↓	Red ↓	Dev ↓	TO ↓
Camera only	1.661	0.73	0.00	0.00	0.14
Left	0.60 ± 0.14	0.00	0.37 ± 0.08	0.19 ± 0.02	0.17
Right	0.47 ± 0.22	0.02 ± 0.04	0.21 ± 0.06	0.20 ± 0.05	0.14 ± 0.07
Front	4.60 ± 0.76	0.42 ± 0.15	0.64 ± 0.20	0.46 ± 0.12	0.24 ± 0.14
Back	0.87 ± 0.18	0.00	0.11 ± 0.07	0.30 ± 0.13	0.11 ± 0.06
No Redact	0.32 ± 0.06	0.00	0.26 ± 0.10	0.00	0.09 ± 0.08

Table 5. Redaction of radar results with Vehicle Infractions (Veh), Static Object Collisions (Stat), Red Light Infractions (Red), Route Deviations (Dev) and Agent Time Outs (TO).

635 Similar results are observed from Table 5 where in the
 636 front radar leads to an unusually high vehicle detection
 637 score, likely due to misclassification. Overall, the model
 638 performs best with all views present, showcasing that each
 639 radar view offers unique contributions, with the front view
 640 essential for vehicle detection and stability.

7. Future Work

641 In future work, we aim to extend our evaluation of C-
 642 Shenron in CARLA by incorporating a more diverse set of
 643 routes from NEAT and other evaluations. Furthermore, we
 644 plan to add effective fusion techniques from multiple views
 645 of radars. We would also like to evaluate more low and
 646 high resolution radars. Additionally, longer and more var-
 647 ied routes will be incorporated to demonstrate the robust-
 648 ness of all community approaches. Expanding the eval-
 649 uation to cover a broader range of towns and conditions
 650 will also allow for more comparisons between our radar-
 651 based model and other state-of-the-art (SOTA) models be-
 652 yond Transfuser++.
 653

References

- 654
- 655 [1] Prashant Ahire, SMM Naidu, Sandeep Varpe, Sakshi
 656 Nadarge, and Anushree Patil. Simulating vehicle driving
 657 using carla. *Journal of Electrical Systems*, 20(10s):44–52,
 658 2024.
 - 659 [2] Mina Alibeigi, William Ljungbergh, Adam Tonderski, Georg
 660 Hess, Adam Lilja, Carl Lindström, Daria Motornik, Jun-
 661 sheng Fu, Jenny Widahl, and Christoffer Petersson. Zenseact
 662 open dataset: A large-scale and diverse multimodal dataset
 663 for autonomous driving. In *Proceedings of the IEEE/CVF*

- 664 *International Conference on Computer Vision*, pages 20178–
665 20188, 2023.
- 666 [3] Kshitiz Bansal, Keshav Rungta, Siyuan Zhu, and Dinesh
667 Bharadia. Pointillism: Accurate 3d bounding box estimation
668 with multi-radars. In *Proceedings of the 18th Conference on*
669 *Embedded Networked Sensor Systems*, pages 340–353, 2020.
- 670 [4] Kshitiz Bansal, Gautham Reddy, and Dinesh Bharadia.
671 Shenron - scalable, high fidelity and efficient radar simu-
672 lation. *IEEE Robotics and Automation Letters*, 9(2):1644–
673 1651, 2024.
- 674 [5] Jens Behley, Martin Garbade, Andres Milioto, Jan Quen-
675 zel, Sven Behnke, Cyrill Stachniss, and Jurgen Gall. Se-
676 mantickitti: A dataset for semantic scene understanding of
677 lidar sequences. In *Proceedings of the IEEE/CVF inter-
678 national conference on computer vision*, pages 9297–9307,
679 2019.
- 680 [6] Dian Chen, Brady Zhou, Vladlen Koltun, and Philipp
681 Krähenbühl. Learning by cheating. In *Conference on Robot*
682 *Learning*, pages 66–75. PMLR, 2020.
- 683 [7] Kashyap Chitta, Aditya Prakash, and Andreas Geiger. Neat:
684 Neural attention fields for end-to-end autonomous driving.
685 In *Proceedings of the IEEE/CVF International Conference*
686 *on Computer Vision*, pages 15793–15803, 2021.
- 687 [8] Kashyap Chitta, Aditya Prakash, Bernhard Jaeger, Zehao Yu,
688 Katrin Renz, and Andreas Geiger. Transfuser: Imitation
689 with transformer-based sensor fusion for autonomous driv-
690 ing. *IEEE Transactions on Pattern Analysis and Machine*
691 *Intelligence*, 45(11):12878–12895, 2022.
- 692 [9] Marius Cordts, Mohamed Omran, Sebastian Ramos, Timo
693 Rehfeld, Markus Enzweiler, Rodrigo Benenson, Uwe
694 Franke, Stefan Roth, and Bernt Schiele. The cityscapes
695 dataset for semantic urban scene understanding. In *Proceed-*
696 *ings of the IEEE conference on computer vision and pattern*
697 *recognition*, pages 3213–3223, 2016.
- 698 [10] CARLA Simulator Developers. Radar sensor model lim-
699 itations in carla simulator. [https://github.com/
700 carla-simulator/carla/issues/4974](https://github.com/carla-simulator/carla/issues/4974), 2024.
- 701 [11] Alexey Dosovitskiy, German Ros, Felipe Codevilla, Antonio
702 Lopez, and Vladlen Koltun. Carla: An open urban driving
703 simulator, 2017.
- 704 [12] Divya Garikapati and Sneha Sudhir Shetiya. Autonomous
705 vehicles: Evolution of artificial intelligence and the current
706 industry landscape. *Big Data and Cognitive Computing*, 8
707 (4):42, 2024.
- 708 [13] Andreas Geiger, Philip Lenz, and Raquel Urtasun. Are we
709 ready for autonomous driving? the kitti vision benchmark
710 suite. In *2012 IEEE conference on computer vision and pat-*
711 *tern recognition*, pages 3354–3361. IEEE, 2012.
- 712 [14] Autonomous Vision Group. Carla garage. [https:
713 //github.com/autonomousvision/carla_
714 garage](https://github.com/autonomousvision/carla_garage), 2024.
- 715 [15] Anthony Hu, Gianluca Corrado, Nicolas Griffiths, Zachary
716 Murez, Corina Gurau, Hudson Yeo, Alex Kendall, Roberto
717 Cipolla, and Jamie Shotton. Model-based imitation learning
718 for urban driving. *Advances in Neural Information Process-*
719 *ing Systems*, 35:20703–20716, 2022.
- [16] Bernhard Jaeger, Kashyap Chitta, and Andreas Geiger. Hid- 720
den biases of end-to-end driving models. In *Proc. of the* 721
IEEE International Conf. on Computer Vision (ICCV), 2023. 722
- [17] Li Li, Khalid N Ismail, Hubert PH Shum, and Toby P 723
Breckon. Durlar: A high-fidelity 128-channel lidar dataset 724
with panoramic ambient and reflectivity imagery for multi- 725
modal autonomous driving applications. In *2021 Interna-* 726
tional Conference on 3D Vision (3DV), pages 1227–1237. 727
IEEE, 2021. 728
- [18] Fei Liu, Zihao Lu, and Xianke Lin. Vision-based environ- 729
mental perception for autonomous driving. *Proceedings of* 730
the Institution of Mechanical Engineers, Part D: Journal of 731
Automobile Engineering, page 09544070231203059, 2022. 732
- [19] Eshed Ohn-Bar, Aditya Prakash, Aseem Behl, Kashyap 733
Chitta, and Andreas Geiger. Learning situational driving. 734
In *Proceedings of the IEEE/CVF Conference on Computer* 735
Vision and Pattern Recognition, pages 11296–11305, 2020. 736
- [20] Quang-Hieu Pham, Pierre Sevestre, Ramanpreet Singh 737
Pahwa, Huijing Zhan, Chun Ho Pang, Yuda Chen, Armin 738
Mustafa, Vijay Chandrasekhar, and Jie Lin. A* 3d dataset: 739
Towards autonomous driving in challenging environments. 740
In *2020 IEEE International conference on Robotics and Au-* 741
tomation (ICRA), pages 2267–2273. IEEE, 2020. 742
- [21] Arvind Srivastav and Soumyajit Mandal. Radars for au- 743
tonomous driving: A review of deep learning methods and 744
challenges. *IEEE Access*, 2023. 745
- [22] Pei Sun, Henrik Kretzschmar, Xerxes Dotiwalla, Aurelien 746
Chouard, Vijaysai Patnaik, Paul Tsui, James Guo, Yin Zhou, 747
Yuning Chai, Benjamin Caine, Vijay Vasudevan, Wei Han, 748
Jiquan Ngiam, Hang Zhao, Aleksei Timofeev, Scott Et- 749
tinger, Maxim Krivokon, Amy Gao, Aditya Joshi, Yu Zhang, 750
Jonathon Shlens, Zhifeng Chen, and Dragomir Anguelov. 751
Scalability in perception for autonomous driving: Waymo 752
open dataset. In *Proceedings of the IEEE/CVF Conference* 753
on Computer Vision and Pattern Recognition (CVPR), 2020. 754
- [23] CARLA Simulator Team. Carla autonomous driving leader- 755
board. <https://leaderboard.carla.org/>, 2024. 756
- [24] Marin Toromanoff, Emilie Wirbel, and Fabien Moutarde. 757
End-to-end model-free reinforcement learning for urban 758
driving using implicit affordances. In *Proceedings of* 759
the IEEE/CVF conference on computer vision and pattern 760
recognition, pages 7153–7162, 2020. 761
- [25] Shanliang Yao, Runwei Guan, Xiaoyu Huang, Zhuoxiao Li, 762
Xiangyu Sha, Yong Yue, Eng Gee Lim, Hyungjoon Seo, 763
Ka Lok Man, Xiaohui Zhu, et al. Radar-camera fusion for 764
object detection and semantic segmentation in autonomous 765
driving: A comprehensive review. *IEEE Transactions on In-* 766
telligent Vehicles, 2023. 767